Available online at www.sciencedirect.com
ScienceDirect
Journal of the European Ceramic Society 30 (2010) 1853–1866
www.elsevier.com/locate/jeurceramsoc

Effect of firing temperature and atmosphere on ceramics made of NW Peloponnese clay sediments: Part II. Chemistry of pyrometamorphic minerals and comparison with ancient ceramics

C. Rathossi [a,*], Y. Pontikes [b,c]

[a] *Section of Earth Materials, Department of Geology, and University of Patras, 26500 Rio, Greece*
[b] *Laboratory of Materials and Metallurgy, Department of Chemical Engineering, University of Patras, 26500 Rio, Greece*
[c] *Department of Metallurgy and Materials Engineering, Katholieke Universiteit Leuven, 3001 Leuven, Belgium*

Received 12 May 2009; received in revised form 26 January 2010; accepted 2 February 2010
Available online 12 March 2010

Abstract

The influence of firing conditions on the chemical composition of the major pyrometamorphic phases of Ca-, Fe-rich Plio-Pleistocene sediments of NW Peloponnese is studied. These sediments have been used in the production of ceramic artefacts for a large historical period and are still in use by the local heavy clay industry. Firing conditions were oxidising (CO/CO_2, %, ranging from 0.2 to 4.4) or reducing atmosphere (CO/CO_2, %, ranging from 11.2 to 23.0), for a temperature range 850–1050 °C. At 850 °C, for both atmospheres, fassaite and gehlenite are the predominant new minerals with anorthite and wollastonite also formed in a small quantity. Up to 950 °C, the chemistry of minerals in oxidising and reducing conditions does not exhibit considerable differences. Fe^{3+} is present even in reducing atmosphere entrapped in the structure of fassaite, gehlenite, anorthite. At 1050 °C, in reducing atmosphere, more hedenbergite component ($CaFe^{2+}Si_2O_6$) incorporates in fassaite, whereas the ferrigehlenite component ($Ca_2Fe_2^{3+}SiO_7$) is absent from gehlenite structure. Fe^{3+} is detected only in fassaite and anorthite structure. The work concludes with a summary of the results from Part I and Part II, in the form of a reverse engineering table for the determination of the firing conditions in a ceramic body by using analytical information. Three examples are given that compare ancient ceramic sherds with ones reproduced in laboratory conditions and demonstrate the effectiveness of this approach.

Keywords: Firing; Microstructure-final; Clays; Traditional ceramics; Archaeometry

1. Introduction

The minerals and their particle size distribution in conjunction with the firing conditions (temperature, atmosphere, soaking time, heating and cooling rate) are the main factors which influence the mineralogical and microstructural transformation during ceramic processing.

Focusing on the firing process, the firing atmosphere has often been neglected as one of the most crucial parameters in determining the final body properties. To provide more experimental work in this area, ceramics were fired in oxidising and reducing atmosphere in a propane-firing kiln. Raw materials were collected from local Plio-Pleistocene sediments, close to Patras, prefecture of Achaia, NW Peloponnese. Excavations in this region have demonstrated an activity of ceramic manufacturing during Archaic (6th c. B.C.), Hellenistic (3rd c. B.C.) and Roman (1st–3rd c. A.D.) period.[1] A number of findings, such as the mineralogy and particle size distribution and most notably the geochemistry between ceramics and clay sediments[2–4] has supported that the collected fine wares have been most probably produced from the clay sediments used in this study without any preparation (e.g. levigation, settling, sieving).

In the previous work, Part I, emphasis was placed on unravelling the high temperature reactions that take place, in the qualitative and quantitative determination of the crystalline phases as well as on the analysis of the microstructure. In the second part presented herein, emphasis is placed on an elaborative microchemical analysis and on the comparison of ancient sherds with replicas prepared under laboratory conditions. The latter signifies one of the main tasks of this work which was to provide

* Corresponding author. Tel.: +30 2610997599; fax: +30 2610997560.
E-mail address: C.Rathosi@upatras.gr (C. Rathossi).

0955-2219/$ – see front matter © 2010 Elsevier Ltd. All rights reserved.
doi:10.1016/j.jeurceramsoc.2010.02.003

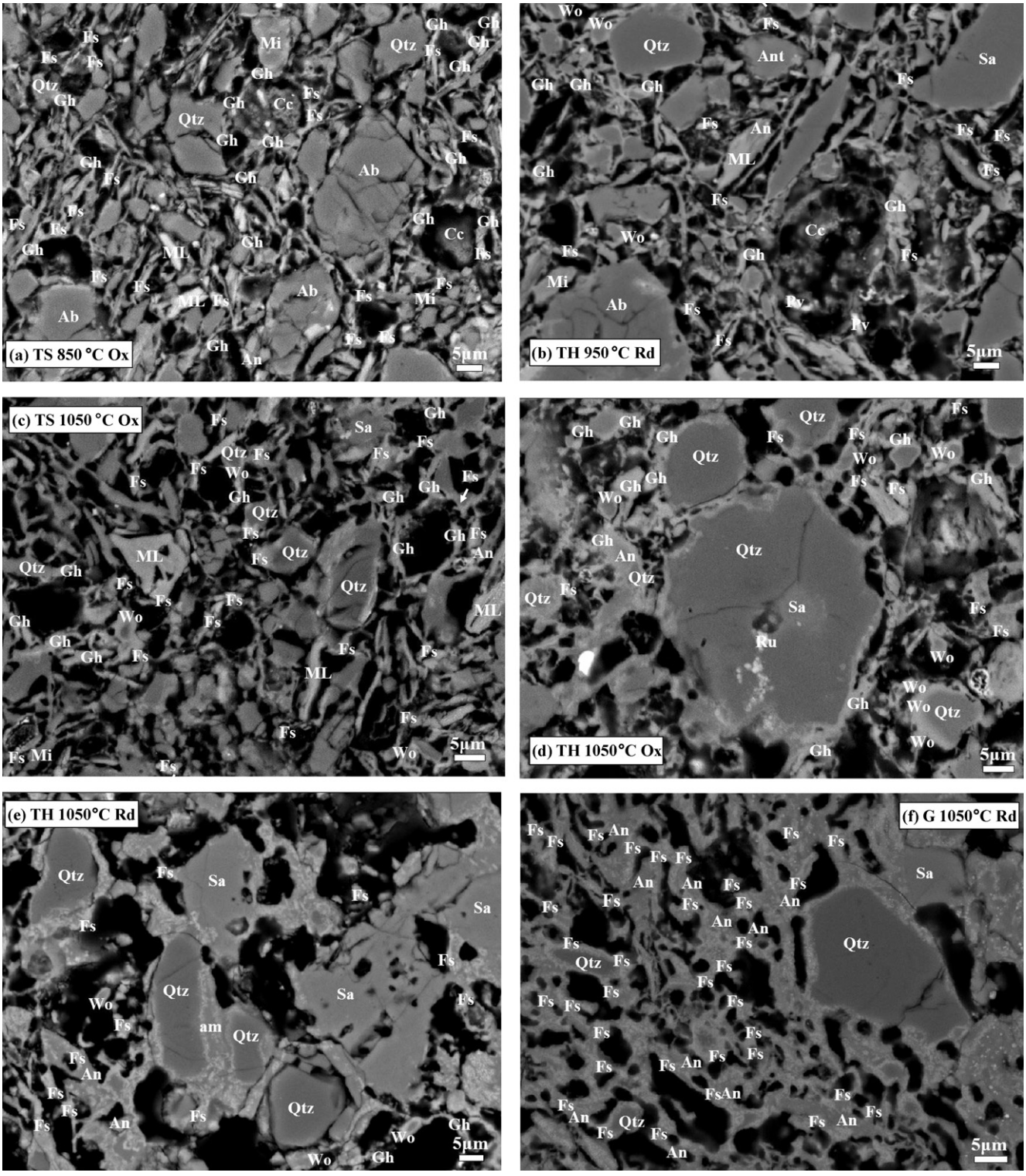

Fig. 1. Backscattered electrons' images of polished surfaces after firing of: (a) TS in oxidising atm., $T = 850\,^{\circ}C$, (b) TH in reducing atm., $T = 950\,^{\circ}C$, (c) TS in oxidising atm., $T = 1050\,^{\circ}C$, (d) TH in oxidising atm., $T = 1050\,^{\circ}C$, (e) TH in reducing atm., $T = 1050\,^{\circ}C$, (f) G in reducing atm., $T = 1050\,^{\circ}C$. *Abbreviations*: Qtz, quartz; Ab, albite; An, anorthite; Sa, sanidine; Fs, fassaite; Gh, gehlenite; Wo, wollastonite; am, amorphous phase; Mi, muscovite; Cc, partially decomposed calcite; Pv, perovskite; Ru, rutile; ML, interstratified muscovite-chlorite.

the tools for a reverse engineering approach: to function as a reference guide after analysis of the ancient body, in order to deduce the firing conditions of the ancient firing and thus duplicate in laboratory conditions (for verification) the ceramic body.

2. Experimental

Three representative raw materials, G, TS and TH, of Plio-Pleistocene sedimentary deposits of NW Peloponnese, have

been used. Detailed information concerning their chemistry, mineralogy, particle size distribution as well as information about the preparation of the samples and the firing is given elsewhere[2,5] and only a summary will be present herein.

Sample TH has the highest CaO content, 14.0wt% approximately, whereas sample G contains the lowest amount of CaO, 9.5wt% approximately, and the highest fraction of clay minerals, 14.0wt% approximately. Remarkable mineralogical differences are not observed; all samples consist of quartz, albite ($NaAlSi_3O_8$), orthoclase ($KAlSi_3O_8$), calcite ($CaCO_3$), white mica (illite/muscovite, $K(Al,Mg,Fe)_2(Si_3,Al)O_{10}(OH)_2$), Fe-rich chlorite ($(Mg,Fe^{2+})_5Al((Al,Si_3)O_{10})(OH)_8$) and mixed-layer clay minerals (white mica/chlorite, chlorite/vermiculite, illite/smectite).

Eighteen specimens were prepared by crushing the raw materials by hand in an agate mortar, mixing with water and shaping the plastic mass in discs, of 5 cm dia. by 1.5 cm height. The discs were dried at room temperature for 5 days, and they were then placed in a resistance oven at 50 °C for 24 h. Firing was performed in a propane-firing kiln. The heating and cooling rate was in all cases 3 °C min^{-1}, firing temperature was 850, 950 and 1050 °C and soaking time was 1 h. The firing atmosphere in gas kiln was controlled by regulating the primary and secondary air flow; Bernoulli-type burners were used. Firing initiated in oxidising atmosphere and the transition to reducing atmosphere, where applicable, took place for T > 800 °C and throughout the soaking period. During cooling, the settings for the burners were not modified initially, however, for T < 800 °C the atmosphere

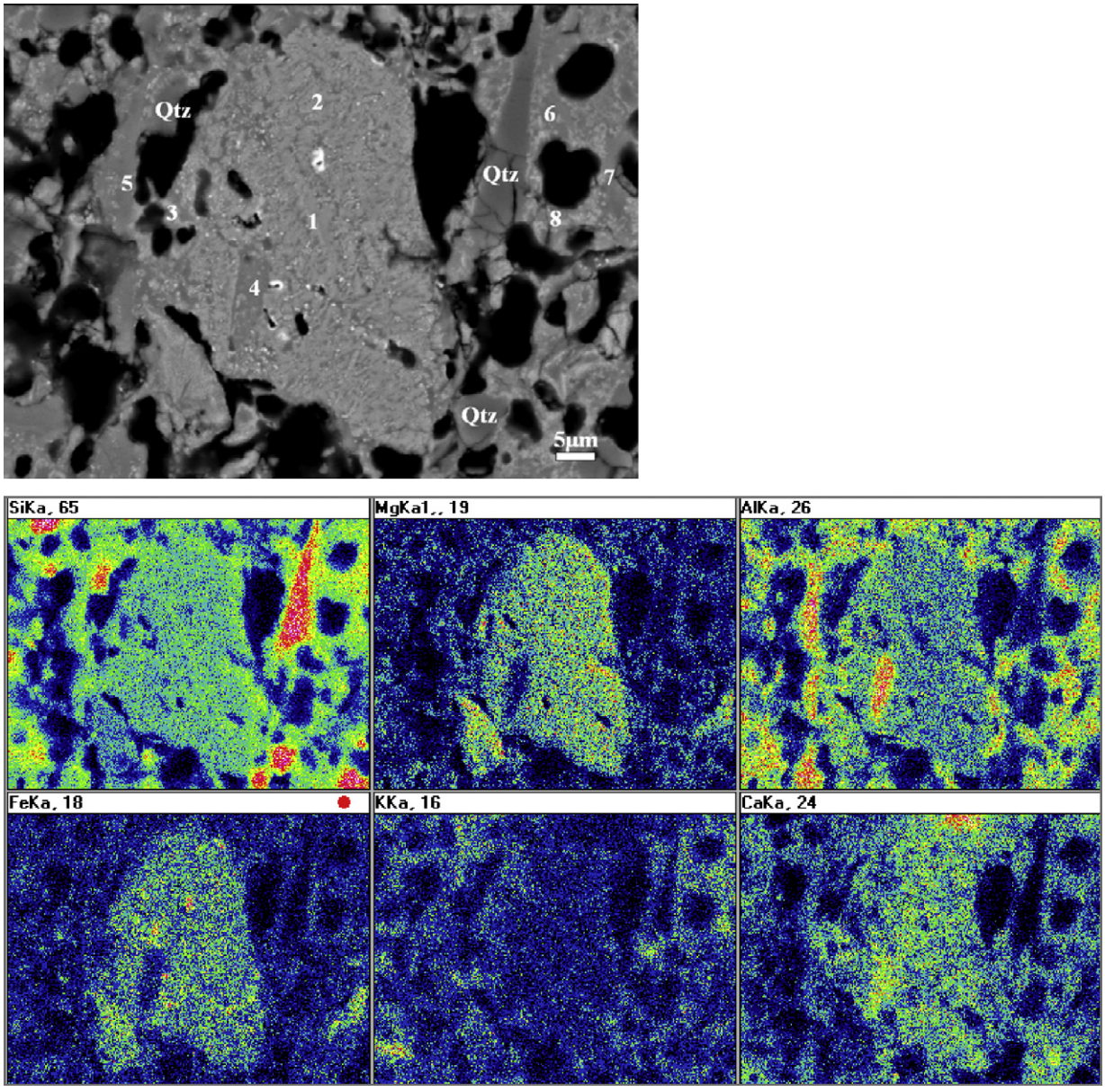

Fig. 2. Elemental mapping on polished surface of TS after firing in reducing atm. at 1050 °C. Top row: secondary electrons' image of the surface, middle row, left to right Si, Mg, Al, bottom row, (left to right) Fe, K, Ca. Spot analyses: aluminium ferroan diopside 1 (Table 2), 2, 3, anorthite 4 (Table 5), labradorite 5, amorphous phase 6–8.

Table 1
Representative EDS-analyses (wt%) and cation proportion (a.p.f.u.) of fassaite crystals in samples fired at 850 and 950 °C in oxidising (ox) and reducing (rd) atmosphere.

	G 850 °C ox	G 950 °C ox	TH 850 °C ox	TH 950 °C ox	TS 850 °C ox	TS 950 °C ox	G 850 °C rd	G 950 °C rd	TH 850 °C rd	TH 950 °C rd	TS 850 °C rd	TS 950 °C rd
SiO_2	38.20	36.33	38.52	32.11	41.11	34.39	42.19	37.58	39.99	35.85	40.11	37.92
TiO_2	1.12	1.53	0.22	–	0.26	0.28	0.42	0.15	–	–	0.25	0.20
Al_2O_3	16.53	16.45	17.51	16.79	17.6	17.7	14.32	19.38	16.28	16.78	16.68	15.99
Fe_2O_3	13.94	14.53	14.52	20.61	14.02	19.20	10.22	13.33	12.56	13.59	15.05	13.95
MnO	–	–	–	–	–	0.21	–	0.67	–	–	0.02	0.23
MgO	5.83	7.06	7.17	5.67	7.08	6.35	8.21	10.78	5.30	9.98	8.08	7.90
CaO	23.44	22.74	21.53	23.81	19.21	20.19	24.23	17.08	24.98	22.48	19.21	22.29
Na_2O	0.67	0.83	0.23	0.35	0.26	0.48	0.23	0.49	0.43	0.71	0.33	0.85
K_2O	0.09	0.51	0.21	0.22	0.33	0.84	0.09	0.50	0.33	0.19	0.16	0.44
Total	99.82	99.98	99.91	99.56	99.87	99.64	99.91	99.96	99.87	99.58	99.89	99.77
Numbers of ions on the basis of 6O												
Si	1.464	1.385	1.467	1.256	1.567	1.333	1.591	1.404	1.527	1.348	1.523	1.438
^{IV}Al	0.536	0.615	0.533	0.744	0.433	0.667	0.409	0.596	0.473	0.652	0.477	0.562
^{VI}Al	0.210	0.124	0.252	0.029	0.356	0.142	0.227	0.257	0.259	0.090	0.269	0.153
Ti	0.032	0.044	0.006	–	0.007	0.008	0.012	0.004	–	–	0.007	0.006
Fe^{3+}	0.344	0.416	0.295	0.606	0.287	0.560	0.198	0.374	0.274	0.384	0.230	0.398
Fe^{2+}	0.064	–	0.133	–	0.127	–	0.102	–	0.096	–	0.223	–
Mg	0.333	0.401	0.407	0.331	0.402	0.367	0.461	0.601	0.302	0.560	0.457	0.447
Mn	–	–	–	–	–	0.007	–	0.021	–	–	0.001	0.007
Ca	0.962	0.929	0.878	0.997	0.784	0.839	0.979	0.684	1.022	0.905	0.782	0.906
Na	0.050	0.061	0.017	0.027	0.019	0.036	0.017	0.035	0.032	0.052	0.024	0.063
K	0.004	0.025	0.010	0.011	0.016	0.042	0.004	0.024	0.016	0.009	0.008	0.021
M1 + M2	1.99	2.00	1.99	2.00	1.99	2.00	2.00	2.00	2.00	2.00	2.00	2.00
$^{VI}Al + Fe^{3+}$	0.554	0.540	0.547	0.635	0.643	0.702	0.425	0.631	0.533	0.474	0.499	0.551
$(Fe^{3+}Al)/(Fe^{2+}Si)$	0.710	0.830	0.680	1.100	0.640	1.030	0.490	0.870	0.620	0.840	0.560	0.770

was inverted to oxidising as there was not practical effect on reduction.

For comparison, ancient ceramic sherds dating from the second half of 1st c. A.D. until the end of 3rd c. A.D. have been used. These sherds represent Roman lamps and derive from two workshops excavated in the city of Patras.[1] The colour of the body was determined by comparison with Munsell soil colour chart. The crystalline phases were identified by X-ray powder diffraction analysis (Bruker D8 Advance, USA) equipped with a LynxEye® detector. Qualitative analysis was performed by the DIFFRAC^{plus} EVA® software (Bruker-AXS, USA) based on the ICDD Powder Diffraction File. The quantification of minerals was carried out using a Rietveld-based quantification routine with the TOPAS® software (DIFFRAC^{plus} TOPAS Ver. 3.0 Tutorial, Bruker-AXS, USA). Details on the X-ray powder diffraction analysis can be retrieved in Part I.[5] The chemical composition of major elements was conducted by inductively coupled plasma-optical emission spectrometry (ICP-OES) at ACTLABS, Ancaster, Ontario, Canada. Detection limit for major elements is 0.01%. The analytical precision calculated from replicate analysis of one sample is better than ±1%.

The chemical analysis of pyrometamorphic crystalline phases was performed on carbon coated thin sections, using scanning electron microscopy, SEM (JEOL 6300, Japan) fitted with an energy dispersive X-ray spectrometer, EDS (LINK PentaFET 6699, Oxford Instruments, U.K.). Natural minerals and synthetic oxides were used as calibration standards.

3. Results and discussion

From 850 °C and for both oxidising and reducing atmospheres, fassaite, gehlenite, anorthite and wollastonite have started to crystallise as XRD patterns reveal.[5] The majority of the EDS-analyses for fassaite and gehlenite at 850 and 950 °C have been performed on a thin rim around pores of pre-existing calcite, where fassaite and gehlenite have been formed as the result of calcite with clay reactions, whereas a smaller number of analyses have been performed within the micromass (Fig. 1a and b). Uncompleted decomposition of calcite grains has been found in all bodies up to 950 °C for both atmospheres (Fig. 1a and b). In sample TH, partially decomposed calcite grains appear more often as a result of higher calcite quantity (approximately 14.0 wt% CaO in the raw mixture) and larger grain size (up to 200 μm). Fassaite and gehlenite were detected also at the edge of fine grained phyllosilicates whereas gehlenite and wollastonite form a very thin rim (up to 2 μm) around boundaries of small quartz grains (Fig. 1a and b). Although the crystallisation of anorthite is inferred at 850 °C from XRD patterns, it has been possible only on a few occasions to be detected by electron microscopy at that temperature, probably due to a very small crystal size.

In both atmospheres at 1050 °C, the white rim in BSE images around pores and the rim around primitive (i.e. originally present) grains is more clearly discernible, implying that the crystal growth of the new phases is enhanced at these conditions (Fig. 1c–f). Compared to oxidation at 1050 °C (Fig. 1c and d),

Table 2
Representative EDS-analyses (wt%) and cation proportion (a.p.f.u.) of fassaite (Fs) and aluminium ferroan diopside (Di) crystals in samples fired at 1050 °C in oxidising (ox) and reducing (rd) atmosphere. The whole database is available after request from the authors.

	G ox Fs	G ox Fs	G ox Fs	TH ox Fs	TH ox Fs	TH ox Fs	TS ox Fs	TS ox Fs	TS ox Fs	G rd Fs	G rd Fs	G rd Di	TH rd Fs	TH rd Fs	TH rd Di	TS rd Fs	TS rd Fs	TS(1) rd Di
SiO_2	41.12	34.93	33.67	40.26	29.59	35.65	40.54	41.99	38.71	46.2	44.18	46.33	47.75	41.02	51.09	50.34	40.45	49.59
TiO_2	0.51	–	0.39	–	–	0.26	–	0.27	–	1.08	–	0.65	0.68	0.59	–	0.34	0.02	0.65
Al_2O_3	14.42	12.67	17.65	16.24	17.57	14.76	17.53	15.32	16.20	8.92	13.19	9.51	8.47	16.57	3.48	3.72	16.31	5.79
Fe_2O_3	14.51	20.21	16.82	15.42	22.43	19.29	12.45	11.31	14.06	14.88	12.98	13.34	12.40	12.37	15.22	13.76	13.6	14.25
MnO	0.28	–	0.39	–	–	–	–	–	–	–	–	0.62	–	–	–	–	–	–
MgO	8.43	8.43	10.37	6.62	6.45	8.24	6.16	7.86	7.45	7.25	6.60	8.26	8.51	6.16	7.82	7.80	8.03	11.15
CaO	19.65	23.53	19.33	20.24	23.18	20.57	21.87	22.31	23.12	20.77	22.55	20.77	20.68	21.94	21.76	23.33	20.73	17.63
Na2O	0.70	–	0.55	1.16	0.45	0.38	0.77	0.54	0.21	0.51	0.32	0.23	0.98	0.85	0.32	0.48	0.40	0.52
K_2O	0.33	–	0.86	–	0.32	0.31	0.65	0.33	0.07	0.31	0.15	0.19	0.42	0.39	0.17	0.25	0.42	0.38
Total	99.95	99.77	100.03	99.94	99.99	99.46	99.97	99.93	99.82	99.92	99.97	99.90	99.89	99.89	99.86	100.02	99.96	99.96
Numbers of ions on the basis of 6O																		
Si	1.560	1.359	1.270	1.531	1.151	1.382	1.533	1.582	1.478	1.773	1.689	1.766	1.808	1.554	1.970	1.935	1.530	1.876
^{IV}Al	0.440	0.580	0.730	0.469	0.805	0.618	0.467	0.418	0.522	0.227	0.311	0.234	0.192	0.446	0.030	0.065	0.470	0.124
^{VI}Al	0.204	–	0.054	0.258	–	0.056	0.314	0.262	0.207	0.176	0.283	0.193	0.186	0.294	0.128	0.104	0.256	0.134
Ti	0.015	–	0.011	–	–	0.008	–	0.008	–	0.031	–	0.019	0.019	0.017	–	0.010	0.001	0.018
Fe^{3+}	0.271	0.591	0.477	0.298	0.656	0.562	0.256	0.211	0.404	0.058	0.258	–	0.085	0.199	–	0.109	0.264	0.028
Fe^{2+}	0.159	–	–	0.159	–	–	0.109	0.122	–	0.413	0.128	0.426	0.298	0.170	0.491	0.322	0.136	0.419
Mg	0.477	0.489	0.583	0.375	0.374	0.476	0.347	0.442	0.424	0.415	0.376	0.469	0.480	0.348	0.450	0.447	0.453	0.629
Mn	0.009	–	0.012	–	–	–	–	–	–	–	–	0.020	–	–	–	–	–	–
Ca	0.799	0.981	0.781	0.825	0.966	0.854	0.886	0.901	0.946	0.854	0.924	0.848	0.839	0.891	0.899	0.961	0.840	0.715
Na	0.051	–	0.040	0.086	0.034	0.029	0.056	0.039	0.016	0.038	0.024	0.017	0.072	0.062	0.024	0.036	0.029	0.038
K	0.016	–	0.041	–	0.016	0.015	0.031	0.016	0.003	0.015	0.007	0.009	0.020	0.019	0.008	0.012	0.020	0.018
M1 + M2	2.00	2.00	1.99	2.00	2.00	2.00	2.00	2.00	2.00	2.00	2.00	2.00	1.99	2.00	2.00	2.00	2.00	1.99
$^{VI}Al + Fe^{3+}$	0.475	0.530	0.531	0.556	0.611	0.618	0.570	0.473	0.611	0.234	0.541	0.193	0.271	0.493	0.128	0.213	0.520	0.162
$(Fe^{3+}Al)/(Fe^{2+}Si)$	0.532	0.861	0.990	0.608	1.269	0.890	0.631	0.522	0.770	0.210	0.468	0.088	0.128	0.544	0.064	0.123	0.594	0.070

Table 3
Representative EDS-analyses (wt%) and cation proportion (a.p.f.u.) of gehlenite crystals in samples fired at 850 and 950 °C in oxidising (ox) and reducing (rd) atmosphere.

	G 850 °C ox	G 950 °C ox	TH 850 °C ox	TH 950 °C ox	TS 850 °C ox	TS 950 °C ox	G 850 °C rd	G 950 °C rd	TH 850 °C rd	TH 950 °C rd	TS 850 °C rd	TS 950 °C rd
SiO_2	30.16	29.19	29.46	31.47	30.46	32.32	31.95	32.20	31.87	36.11	30.70	32.93
TiO_2	–	0.15	–	0.45	–	0.56	–	0.74	–	–	0.79	–
Al_2O_3	18.79	17.11	18.64	16.34	16.13	16.04	17.97	15.60	17.32	12.95	20.23	17.63
FeO	7.67	9.00	8.96	6.94	9.97	6.91	4.87	7.13	7.69	6.53	5.23	4.80
MnO	–	0.30	–	0.30	–	–	–	–	–	–	–	–
MgO	3.48	4.77	3.13	4.88	3.84	4.13	4.89	4.71	3.55	5.00	3.31	3.90
CaO	38.10	38.39	39.77	38.87	38.98	39.54	39.55	38.68	39.33	38.38	39.09	38.47
Na_2O	0.80	0.34	–	0.13	0.34	0.27	0.35	0.61	0.11	0.67	0.52	0.77
K_2O	–	0.42	–	0.51	0.09	–	–	0.21	0.02	0.27	–	0.42
Total	99.00	99.67	99.96	99.89	99.81	99.77	99.58	99.88	99.89	99.91	99.87	99.92
Numbers of ions on the basis of 14O												
Si	2.834	2.759	2.785	2.949	2.899	3.031	2.970	3.023	2.992	3.371	2.852	3.069
Al	2.079	1.905	2.075	1.803	1.808	1.771	1.967	1.725	1.915	1.424	2.213	1.935
Ti	–	0.011	–	0.032	–	0.040	–	0.052	–	–	0.055	–
Fe^{2+}	–	–	0.316	0.157	0.398	0.307	0.155	0.324	0.393	0.510	0.233	0.374
Fe^{3+}	0.542	0.640	0.352	0.348	0.356	0.212	0.201	0.212	0.190	–	0.156	0.070
Mn	–	0.024	–	0.024	–	–	–	–	–	–	–	–
Mg	0.487	0.672	0.441	0.682	0.545	0.577	0.678	0.659	0.497	0.696	0.458	0.542
Ca	3.836	3.888	4.028	3.903	3.975	3.973	3.939	3.891	3.956	3.839	3.891	3.841
Na	0.146	0.062	–	0.024	0.063	0.049	0.063	0.111	0.020	0.121	0.094	0.139
K	–	0.051	–	0.061	0.011	–	–	0.025	0.002	0.032	–	0.050
Cations	9.924	10.012	9.997	9.983	10.055	9.960	9.973	10.022	9.965	9.993	9.952	10.020

more amorphous phase, crowded with crystal nuclei, develops in reducing atmosphere (Fig. 1e and f). The elemental mapping of TS fired in reduction at 1050 °C, Fig. 2, provides insight in the neomineralisation which took place after the diffusion of CaO and the structural breakdown of the interstratified chlorite-white mica phyllosilicate grain (centre of the image, enrichment mainly in Mg, Fe, Si, Al and to a lesser extent in K), with or without the participation of quartz (reactions (4), (7) and (8) in Part I[5]). The newly formed minerals are: Ca-rich plagioclase (anorthite), analyses 1, 2, high level in Ca, Al, Si; aluminium fer-

Table 4
Representative EDS-analyses (wt%) and cation proportion (a.p.f.u.) of gehlenite crystals in samples fired at 1050 °C. The whole database is available after request from the authors.

	G ox	G ox	G ox	TH ox	TH ox	TH ox	TS ox	TS ox	TS ox	G rd	G rd	G rd	TH rd	TH rd	TH rd	TS rd	TS rd	TS rd
SiO_2	32.45	29.19	30.18	33.45	29.36	29.43	30.62	30.09	33.21	30.99	33.09	33.59	34.17	32.81	35.82	31.57	33.63	34.12
TiO_2	–	0.15	–	–	–	–	0.20	0.28	0.45	0.41	–	–	–	–	–	–	–	–
Al_2O_3	15.88	17.11	16.99	11.09	17.59	15.58	15.48	13.95	15.48	18.35	15.24	17.83	16.85	19.81	14.13	19.88	17.15	15.64
FeO	6.25	9.00	10.7	11.61	10.38	11.59	9.59	10.90	6.86	7.93	6.44	4.08	4.66	4.61	5.43	5.66	4.56	5.98
MnO	0.35	0.30	–	–	–	0.41	–	–	–	–	–	–	–	–	–	–	–	–
MgO	5.25	4.77	2.54	4.70	2.38	4.65	4.65	5.56	4.65	2.26	5.02	4.08	3.97	2.73	4.63	2.87	4.75	4.59
CaO	38.88	38.39	39.47	39.09	39.02	37.61	38.97	37.63	38.61	39.15	40.08	40.40	39.52	38.97	40.00	39.92	39.26	39.62
Na_2O	0.42	0.34	–	–	–	0.30	0.30	0.39	0.41	0.15	–	–	0.49	0.49	–	–	0.49	–
K_2O	0.31	0.42	–	–	–	0.45	0.15	0.84	0.12	0.10	–	–	–	0.27	–	–	–	–
Total	99.79	99.67	99.88	99.94	98.73	100.00	99.96	99.64	99.79	99.34	99.87	99.98	99.66	99.69	100.01	99.9	99.84	99.95
Numbers of ions on the basis of 14O																		
Si	3.032	2.759	2.872	3.191	2.834	2.791	2.892	2.864	3.103	2.947	3.110	3.104	3.173	3.042	3.323	2.945	3.118	3.181
Al	1.747	1.905	1.904	1.246	2.000	1.740	1.722	1.564	1.704	2.055	1.687	1.941	1.843	2.163	1.544	2.184	1.872	1.717
Ti	–	0.011	–	–	–	–	0.014	0.020	0.032	0.029	–	–	–	–	–	–	–	–
Fe^{2+}	0.156	–	0.398	0.479	0.515	–	0.158	–	0.313	0.631	0.506	0.315	0.362	0.358	0.421	0.442	0.354	0.466
Fe^{3+}	0.299	0.640	0.408	0.402	0.290	0.826	0.539	0.780	0.201	–	–	–	–	–	–	–	–	–
Mn	0.028	0.024	–	–	–	0.033	–	–	–	–	–	–	–	–	–	–	–	–
Mg	0.731	0.672	0.360	0.668	0.342	0.657	0.655	0.789	0.648	0.320	0.703	0.562	0.550	0.377	0.640	0.399	0.656	0.638
Ca	3.892	3.888	4.025	3.996	4.036	3.821	3.944	3.837	3.866	3.989	4.036	4.000	3.932	3.872	3.975	3.990	3.899	3.957
Na	0.076	0.062	–	–	–	0.055	0.055	0.072	0.074	0.028	–	–	0.088	0.088	–	–	0.088	–
K	0.037	0.051	–	–	–	0.054	0.018	0.102	0.014	0.012	–	–	–	0.032	–	–	–	–
Cations	9.998	10.012	9.967	9.982	10.017	9.977	9.997	10.028	9.955	10.011	10.042	9.922	9.948	9.932	9.903	9.960	9.987	9.959

Table 5
Representative EDS-analyses (wt%) and cation proportion (a.p.f.u.) of anorthite and wollastonite crystals in samples fired at 1050 °C.

Sample	G	TH	TS	G	TH	TS	G	TH	TS	G	TH	TS
Atm	ox	ox	ox	rd	rd	rd	ox	ox	ox	rd	rd	rd
Mineral	An	An	An	An	An	An	Wo	Wo	Wo	Wo	Wo	Wo
SiO_2	47.71	49.34	44.36	43.82	45.73	48.54	47.68	47.88	49.19	50.59	50.95	49.95
TiO_2	–	–	–	–	–	0.20	–	–	–	–	–	–
Al_2O_3	29.95	28.24	31.02	31.99	32.75	31.18	4.21	3.31	2.98	1.41	0.94	1.29
Fe_2O_3	1.19	3.29	1.01	2.22	2.16	0.57	–	–	–	–	–	–
FeO	–	–	–	–	–	–	2.11	0.92	1.21	0.85	0.70	2.14
MnO	–	–	–	–	–	–	–	–	–	–	–	–
MgO	0.13	1.29	1.81	0.84	0.39	0.19	1.38	1.11	0.78	0.79	0.63	–
CaO	19.17	15.19	18.8	19.61	17.36	17.2	44.41	45.35	45.73	45.98	46.8	46.04
Na_2O	1.13	1.46	1.80	0.98	0.99	1.23	–	0.33	–	–	–	–
K_2O	0.69	1.03	0.82	0.46	0.65	0.60	–	0.12	–	–	–	0.38
Total	99.97	99.84	99.62	99.92	100.03	99.71	99.79	99.02	99.89	99.62	100.02	99.80
Numbers of ions on the basis of 32O									Numbers of ions on the basis of 18O			
Si	8.877	9.148	8.359	8.238	8.490	8.955	5.565	5.632	5.719	5.882	5.908	5.856
Al	6.562	6.166	6.884	7.082	7.160	6.775	0.579	0.459	0.408	0.193	0.128	0.178
Fe^{3+}	0.166	0.459	0.143	0.314	0.301	0.079	–	–	–	–	–	–
Fe^{2+}	–	–	–	–	–	–	0.206	0.091	0.118	0.083	0.068	0.210
Ti	–	–	–	–	–	0.028	–	–	–	–	–	–
Mn	–	–	–	–	–	–	–	–	–	–	–	–
Mg	0.036	0.357	0.508	0.235	0.108	0.052	0.240	0.195	0.135	0.137	0.109	–
Ca	3.821	3.017	3.796	3.950	3.453	3.400	5.554	5.716	5.696	5.727	5.814	5.783
Na	0.408	0.525	0.658	0.357	0.356	0.440	–	0.075	–	–	–	–
K	0.164	0.244	0.197	0.110	0.154	0.141	–	0.018	–	–	–	0.057
Cations	20.034	19.916	20.545	20.286	20.022	19.870	12.140	12.186	12.080	12.020	12.030	12.084
Ab	9.3	13.9	14.1	8.1	9.0	11.1						
An	87.0	79.7	81.6	89.4	87.1	85.4						
Or	3.7	6.4	4.2	2.5	3.9	3.5						

roan diopside, analyses 3–5, high level in Fe, Mg, Al; Fe-oxides, high level only in Fe. Potassium (K) from the mica structure has diffused in the micromass. At the right area, around the quartz grain, the structure seems amorphous based on the morphology and the composition: 57–59 wt% SiO_2, 9–18 wt% Al_2O_3, 3–9 wt% FeO, 1–4 wt% MgO, 8–13 wt% CaO, 1.5–5 wt% K_2O and 1–3 wt% Na_2O.

Representative chemical analyses for new minerals crystallised at 850, 950 and 1050 °C, are presented in Tables 1–5. The reported data cover only the minerals that had a crystal size

Table 6
Summary report of firing properties of Plio-Pleistocene sediments with CaO content between 5 and 10 wt%. Firing is for 1 h soaking time and slow cooling. Ox: oxidising atm.; rd: reducing atm. For the abbreviation of the minerals see caption of Fig. 1.

Property	Analytical result	Firing properties
Macroscopic colour in fired body	Reddish yellow	850 °C ox/rd
		950 °C ox
	Light brown	950 °C rd
		1050 °C ox
	Brown/yellowish brown	1050 °C rd
Mineralogical quantification	Fs > Gh > An ∼ Wo	850 °C ox/rd (not-reacted Cc)
		950 °C ox/rd (if Mt > He then rd)
	An ∼ Fs > Wo > Gh	1050 °C ox
	An > Fs > Wo > Gh, Qtz reduced, Gh < 1.5 wt%	1050 °C rd
Microchemistry	$Fe^{3+} > Fe^{2+}$ in Fs, Gh	850/950/1050 °C ox
		850/950 °C rd
	$Fe^{3+} \leq Fe^{2+}$ in Fs No Fe^{3+} in Gh	1050 °C rd
Microstructure	Open, interconnected porosity	850–950 °C ox/rd
	Open and closed pores	1050 °C ox
	Large, spherical, closed pores, vitrification, rounded and diffusive Qtz	1050 °C rd

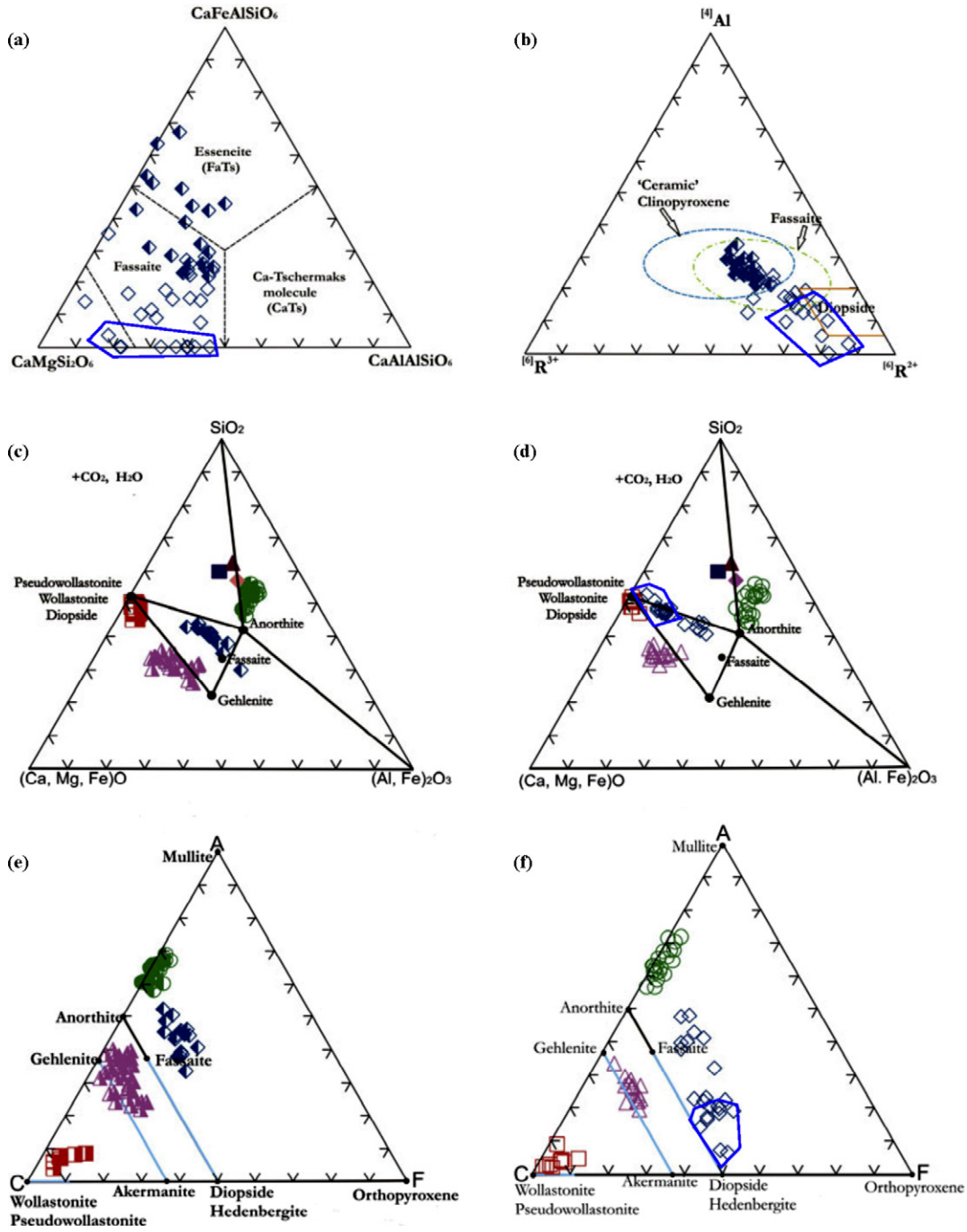

Fig. 3. Plot of fassaite composition in the ternary diagram (a) diopside-Ca-Tschermakite-esseneite[10] and (b) $^{[4]}Al$–$^{[6]}R^{3+}$–$^{[6]}R^{2+}$ composition fields of natural fassaite, diopside[39] and 'ceramic' clinopyroxenes.[40] Fassaite, gehlenite, anorthite and wollastonite composition in the ternary diagram (Ca, Mg, Fe)O–(Al, Fe)$_2$O$_3$–SiO$_2$ (c) in oxidation, (d) in reduction, and in ACF diagram (e) in oxidation, (f) in reduction. Raw materials composition (TS: full triangle; TH: full square; and G: full rhomb) are plotted in diagram (c) and (d). Key for symbols, rhomb: fassaite and aluminium ferroan diopside (the marked area); triangle: gehlenite; circle: anorthite; square: wollastonite (half: oxidising atm., open: reducing atm.).

sufficiently large (to minimise contribution by adjacent mineral phases) for reliable chemical analyses. In those events where the number of reliable chemical analyses is sufficiently high, the average chemical formula and the lattice parameters are also reported.

The discussion that follows provides details for the clinopyroxene$_{ss}$, melilite$_{ss}$, plagioclase$_{ss}$ and wollastonite.

Clinopyroxene$_{ss}$: At three temperatures in oxidising firing and at 850 and 950 °C in reduction, the unit-cell parameters refined by least-squares using the powder-diffraction data range as: a (Å) = 9.721(4)–9.738(2), b (Å) = 8.847(4)–8.865(3), c (Å) = 5.297(2)–5.302(1), β (°) = 106.30(3)–106.08(2) and V (Å^3) = 436.78(3)–440.05(1). In reducing firing at 1050 °C the unit-cell parameters slightly differentiate, as follows:

Table 7
Summary report of firing properties of Plio-Pleistocene sediments with a CaO content ranges between 10 and 15 wt%. Firing is for 1 h soaking time and slow cooling. Ox: oxidising atm.; rd: reducing atm. For the abbreviation of the minerals see caption of Fig. 1.

Property	Analytical result	Firing properties
Macroscopic colour in fired body	Light brown	850 °C ox/rd
	Very pale brown	950 °C ox/rd
		1050 °C ox
	Pale yellow	1050 °C rd
Mineralogical Quantification	Fs ~ Gh > Wo > An	850 °C ox/rd (not-reacted Cc)
		950 °C ox/rd (if Mt > He then rd)
	Fs > An > Wo ~ Gh	1050 °C ox
	Fs > An > Wo > Gh	1050 °C rd
	Qtz reduced	
Microchemistry	$Fe^{3+} > Fe^{2+}$ in Fs, Gh	850/950/1050 °C ox
		850/950 °C rd
	$Fe^{3+} \leq Fe^{2+}$ in Fs	1050 °C rd
	No Fe^{3+} in Gh	
Microstructure	Open, interconnected porosity	850–950 °C ox/rd
	Open and closed pores	1050 °C ox
	Large, spherical, closed pores, vitrification, rounded & diffusive Qtz	1050 °C rd

a (Å) = 9.737(2), b (Å) = 8.889(1), c (Å) = 5.278(5), β (°) = 106.14(1) and V (Å^3) 438.44(2).

In all cases these data are in excellent agreement with the cell parameters of a synthetic fassaitic clinopyroxene, which main components are $CaMgSi_2O_6$ (Di, diopside molecule), $CaAl_2SiO_6$ (CaTs, Ca-Tschermak's molecule) and $CaFe^{3+}AlSiO_6$ (Ess, esseneite molecule).[6,7,11,12,14,15,18] Clinopyroxene is characterised by two tetrahedral positions (T) and two octahedral sites (M1 regular and M2 distorted) per formula. In fassaite (or "ferrian aluminian diopside" according to the International Mineralogical Association's Commission on New Mineral Names[8]), the Si deficiency in T site is compensated by the presence of Al between 0.25 and 0.50 per mole. In addition, a high content of aluminium and ferric iron is placed into the M1 site whereas the M2 position is occupied almost entirely by Ca (CaO approximately 25 wt%).[9,10] The esseneite and Ca-Tschermak's substitution may be represented by the replacement (Mg, Fe^{2+})Si ⇔ (Al, Fe^{3+})Al (Fig. 3a). Therefore, an increase in either molecular content of $CaFe^{3+}AlSiO_6$ or $CaAl_2SiO_6$, results to a decrease in the b-dimension, which is caused by the substitution of Fe^{3+} or Al for Mg in octahedral sites, and an increase in the c-dimension, which results from the replacement of Si by Al in tetrahedral sites.[7,11–15]

In oxidising atmosphere, the EDS-analyses indicated that the composition of clinopyroxene$_{ss}$ crystals vary within a broad range. All analyses were normalized to six oxygens and recalculated to four cations, assuming all iron to be in ferric state. The ferrous iron was estimated by charge balance[16] and the end-member components were recalculated according to Cawthorn and Collerson.[17] The presence of aluminium in tetrahedral coordination compensates the Si deficiency (1.15–1.64 a.p.f.u.) and its content ranges from 0.36–0.80 a.p.f.u. All Fe^{3+} is indicated to be placed in octahedral sites, $Al^{VI} + Fe^{3+}$ in M1 positions range from 0.18 to 0.98 a.p.f.u. The Mg and Fe^{2+} range between 0.20–0.63 and 0.00–0.39 a.p.f.u. respectively, occupying both M1 and M2 sites. However, the M2 sites are almost completely taken by Ca (0.78–1.02 a.p.f.u.). Due to the high Fe^{3+}/Fe^{2+} ratios, the composition of clinopyroxene$_{ss}$ ranges from fassaite to esseneite (avr. Tschermak's content, $Di_{43}CaTs_{24}Ess_{33}$ for analysed crystals at 850 °C and $Di_{42}CaTs_{20}Ess_{38}$ at 950 and 1050 °C respectively, Tables 1 and 2, Fig. 3a–c and e). The presence of K in the structure is incompatible with the pyroxene structure and is attributed to contamination.

Table 8
Macroscopic observation of colour for Roman lamp shreds according to Munsell soil colour chart.

PY2	7.5YR 6/6 reddish yellow
PY12	10YR 7/4 very pale brown
PBY10	5Y 7/3 pale yellow

At 850 °C, the average chemical formula is $(Ca_{0.91}Na_{0.03}K_{0.01}Fe^{2+}_{0.03}Mg_{0.02})(Mg_{0.38}Fe^{2+}_{0.08}Fe^{3+}_{0.30}Al_{0.23}Ti_{0.01})(Si_{1.48}Al_{0.52})O_6$, and at 950, 1050 °C is $(Ca_{0.91}Na_{0.04}K_{0.01}Fe^{2+}_{0.02}Mg_{0.02})(Mg_{0.38}Fe^{2+}_{0.06}Fe^{3+}_{0.37}Al_{0.18}Ti_{0.01})(Si_{1.46}Al_{0.54})O_6$.

The solubility of esseneite component in the fassaite's structure is strongly affected by the variation of oxygen fugacity and temperature and it is not influenced by pressure. Thus, the high molecular content of esseneite suggests fO_2 values approaching or slightly exceeding the buffer of hematite–magnetite.[7,13,18–21]

Fassaitic clinopyroxene is also formed at 850 and 950 °C in reduction (Table 1). The composition at 850 °C is similar to that in oxidation, $Di_{43}CaTs_{24}Ess_{33}$, while at 950 °C the increase of Ess (approximately 34 mol%), is lower than that in oxidising atmosphere for the same firing temperature ($Di_{44}CaTs_{22}Ess_{34}$, avr. structural formula $(Ca_{0.90}Na_{0.03}K_{0.01}Fe^{2+}_{0.02}Mg_{0.04})(Mg_{0.41}Fe^{2+}_{0.02}Fe^{3+}_{0.34}Al_{0.22}Ti_{0.01})(Si_{1.46}Al_{0.54})O_6$). Noteworthy changes in the composition of clinopyroxene$_{ss}$ were observed at 1050 °C in reduction. Two different chemical compositions of clinopyroxene$_{ss}$ may be distinguished. The first type of clinopyroxene$_{ss}$ has an average chemical formula

Table 9
Concentration in wt% for the major elements of Roman lamp shreds.

	SiO_2	Al_2O_3	Fe_2O_3	MnO	MgO	CaO	Na_2O	K_2O	TiO_2	P_2O_5	LOI	Total
PY2	59.45	13.21	5.74	0.103	2.91	9.35	1.48	2.54	0.740	0.25	4.38	100.14
PY12	54.76	14.22	6.58	0.115	3.38	11.08	1.36	2.69	0.777	0.20	4.87	100.03
PBY10	56.26	14.23	6.48	0.120	3.44	12.20	1.35	2.50	0.762	0.42	2.44	100.20

Table 10
Rietveld-based quantification analysis of Roman lamp shreds PY2, PY12 and PBY10 in wt%. The numbers in parentheses declare the quantification errors; b.d.l.: below detection limits; GOF: "Goodness of Fit" = $\chi^2 = R_{wp}/R_{exp}$, see Part I for details. *Abbreviations*: Qtz: quartz, An: anorthite (An_{75-100}), Ab: albite (An_{0-50}), Sa: sanidine (>Or_{44}), Ant: anorthoclase (<Or_{25}), Fs: fassaite (Fe^{3+}, Al-rich clinopyroxene), Gh: gehlenite, He: hematite, Mt: magnetite, Wo: wollastonite, Fo: ferroan forsterite, SCc: secondary calcite. The estimated firing temperature and atmosphere is also given.

Samples	Temp. (°C)/Atm	Qtz	Plg_1	Plg_2	Sa	Ant	Fs	Gh	He	Mt	Wo	Fo	SCc	Amorph.	GOF
PY2	~900–950 °C/oxidising atm	27.4(8)	7.5(1)	11.6(4)	11.9(5)	1.3(7)	14.6(6)	4.9(3)	1.8(1)	1.1(2)	4.9(5)	2.9(5)	8.5(3)	1.6	1.18
PY12	~1000–1050 °C/oxidising atm	22.1(1)	16.5(1)	10.8(1)	10.8(5)	4.8(2)	19.3(9)	3.3(3)	0.7(1)	2.8(2)	1.7(2)	2.6(7)	3.5(2)	1.1	1.24
PBY10	~1050–1100 °C/reducing atm	11.8(3)	26.1(5)	8.4(4)	2.9(4)	2.5(6)	30.4(8)	0.2(1)	b.d.l.	2.2(1)	2.9(3)	2.2(6)	b.d.l.	10.4	1.15

Table 11
Representative EDS-analyses (wt%) and cation proportion (a.p.f.u.) of fassaite (Fs) and gehlenite (Gh) crystals in ancient ceramic shreds (Roman lamps).

Anc. Ceram.	PY2	PY2	PY12	PY12	PBY10	PBY10		PY2	PY12	PBY10
T °C	950	950	1050	1050	1050	1050		950	1050	1050
Atm	ox	ox	ox	ox	rd	rd		ox	ox	rd
Mineral	Fs	Fs	Fs	Fs	Fs	Fs		Gh	Gh	Gh
SiO_2	37.48	40.82	29.22	41.14	43.56	41.00	SiO_2	29.89	33.55	33.14
TiO_2	0.79	–	–	–	0.75	0.49	TiO_2	–	–	–
Al_2O_3	16.17	16.59	15.78	16.39	13.73	14.37	Al_2O_3	16.22	12.77	16.98
Fe_2O_3	15.08	13.28	22.8	8.40	11.8	13.66	FeO	9.62	10.25	5.99
MnO	–	–	–	–	–	–	MnO	–	–	–
MgO	7.22	7.55	8.22	6.15	6.51	7.73	MgO	5.12	4.11	3.78
CaO	22.46	20.84	23.41	20.78	22.39	21.67	CaO	38.22	38.18	38.68
Na_2O	0.47	0.39	0.19	0.70	0.72	0.59	Na_2O	0.60	0.61	0.80
K_2O	0.27	0.31	0.11	0.30	0.37	0.33	K_2O	0.07	0.19	–
Total	99.94	99.78	99.73	99.86	99.83	99.84	Total	99.74	99.66	99.37
Numbers of ions on the basis of 6 O							Numbers of ions on the basis of 14O			
Si	1.434	1.548	1.137	1.568	1.654	1.557	Si	2.817	3.190	3.110
^{IV}Al	0.566	0.452	0.723	0.432	0.346	0.443	Al	1.800	1.430	1.877
^{VI}Al	0.163	0.288	–	0.304	0.269	0.199	Ti	–	–	–
Ti	0.023	–	–	–	0.021	0.014	Fe^{2+}	–	0.477	0.470
Fe^{3+}	0.434	0.236	0.667	0.241	0.137	0.228	Fe^{3+}	0.682	0.304	–
Fe^{2+}	–	0.159	–	0.191	0.222	0.180	Mn	–	–	–
Mg	0.462	0.427	0.477	0.349	0.369	0.438	Mg	0.719	0.583	0.529
Mn	–	–	–	–	–	–	Ca	3.860	3.889	3.890
Ca	0.921	0.847	0.976	0.849	0.911	0.882	Na	0.110	0.112	0.146
Na	0.035	0.029	0.014	0.052	0.053	0.043	K	0.008	0.023	–
K	0.013	0.015	0.005	0.015	0.018	0.016	Cations	9.996	10.008	10.022
M1+M2	2.05	2.00	2.14	2.00	2.00	2.00				
$^{VI}Al+Fe^{3+}$	0.620	0.524	0.667	0.545	0.427	0.441				
$(Fe^{3+}Al)/(Fe^{2+}Si)$	0.237	0.195	0.264	0.199	0.161	0.168				

$(Ca_{0.88}Na_{0.04}K_{0.01}Mn_{0.00}Fe^{2+}_{0.05}Mg_{0.02})(Mg_{0.41}Fe^{2+}_{0.19}Fe^{3+}_{0.15}Al_{0.23}Ti_{0.02})(Si_{1.69}Al_{0.31})O_6$, and is relevant to fassaite in oxidising atmosphere (avr. Tschermak's content, $Di_{52}CaTs_{30}Ess_{18}$). However, in this case the replacement of Si^{IV} by Al^{IV} in tetrahedral coordination is reduced, ranging from 0.14 to 0.47 a.p.f.u., $Al^{VI} + Fe^{3+}$ in octahedral coordination range from 0.16 to 0.61 a.p.f.u. and the Fe^{3+}/Fe^{2+} ratio is reduced, as Fe^{2+} occupies more sites than Fe^{3+} in M1 position (avr. Tschermak's content, $Di_{52}CaTs_{30}Ess_{18}$, Table 2, Fig. 3a, b, d and f). The lower ratio $(Fe^{3+}Al)/(Fe^{2+}Si)$, suggests that the esseneite component (Ess, $CaFe^{3+}AlSiO_6$) is replaced by more hedenbergite component (Hd, $CaFe^{2+}Si_2O_6$), leading to an increase in *b*-dimension and a decrease in *c*-dimension in the unit-cell parameters, while the fO_2 seems to be controlled by the hematite–magnetite (HM) and quartz–fayalite–magnetite (QFM) buffers.[10,12–14] The replacement of esseneite by hedenbergite molecule results gradually in changes in the nature of clinopyroxene$_{ss}$. A second chemical composition appears to be close to an aluminium ferroan diopside (Table 2 and also the marked areas in Fig. 3) with an average formula

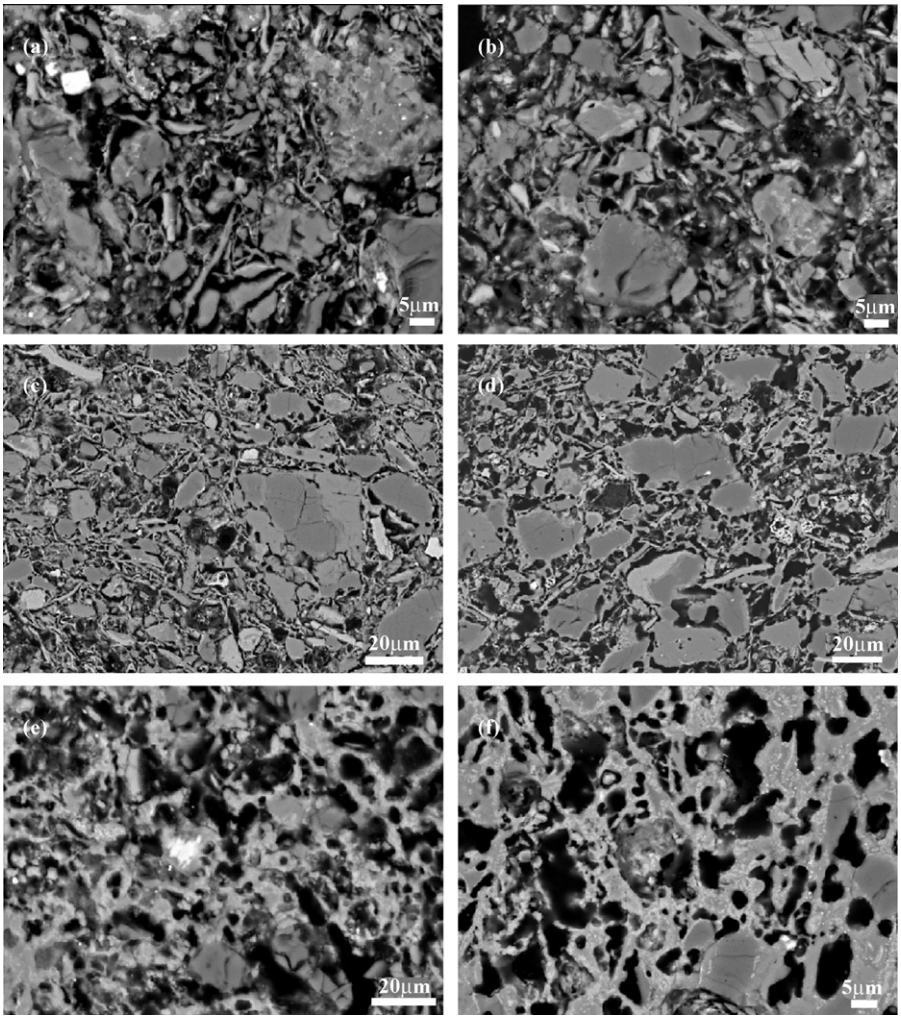

Fig. 4. Backscattered electrons' images of polished surfaces. Left column presents Roman lamps' shreds: (a) PY2, (c) PY12, (e) PBY10 (for information about estimated firing temperature and atmosphere see Table 8). Right column presents clay samples produced at laboratory: (b) TS (oxidising atm., $T = 950\,^{\circ}C$), (d) TH (oxidising atm, $T = 1050\,^{\circ}C$), (f) TS (reducing atm., $T = 1050\,^{\circ}C$).

$(Ca_{0.90}Na_{0.04}K_{0.02}Fe^{2+}_{0.04})(Mg_{0.40}Fe^{2+}_{0.36}Al_{0.22}Ti_{0.02})(Si_{1.85}Al_{0.15})O_6$ and all iron incorporated in the structure as Fe^{2+}.

Melilite$_{ss}$: In both atmospheres, the lattice parameters indicated a solid solution ranging in composition between gehlenite and åkermanite with gehlenite to predominate.[22–27] At 850 and 950 °C the cell-dimensions of melilite$_{ss}$ are: a (Å) = 7.714(2), c (Å) = 5.075(1), V (Å^3) = 302.09(2) in samples G and TS and a (Å) = 7.731(1), c (Å) = 5.051(1), V (Å^3) = 302.11(1) in sample TH. In oxidising at 1050 °C, the unit-cell parameters are slightly changed: a (Å) = 7.708(5), c (Å) = 5.057(6), V (Å^3) = 301.18(6) for crystals formed in samples G and TS and a (Å) = 7.742(1), c (Å) = 5.048(2), V (Å^3) = 302.67(1) for crystals in sample TH. In reducing atmosphere, the lattice parameters are: a (Å) = 7.726(2), c (Å) = 5.046(3), V (Å^3) = 301.99(2). Decrease of the gehlenite content in the solid solution results to an increase of the a-dimension and a decrease of the c-dimension.[28–30]

EDS-analyses gave more detailed results for the incorporation of end-members in the formed solid solution. All analyses were normalized to fourteen oxygens and recalculated to ten cations assuming all iron to be in ferrous state; the ferric iron was estimated by charge balance[16] (Tables 3 and 4, Fig. 3c and e). In oxidising atmosphere the melilite$_{ss}$ crystals are a solid solution involving the end-members gehlenite $Ca_2Al_2SiO_7$ and ferrigehlenite $Ca_2Fe^{3+}_2SiO_7$ in addition to åkermanite $Ca_2MgSi_2O_7$ and ferroåkermanite $Ca_2Fe^{2+}Si_2O_7$. The molecular content of end-members is $Geh_{54}FGeh_7Åk_{26}FÅk_{12}$ for crystals formed at 850 and 950 °C (avr. chemical formula $(Ca_{1.95}Na_{0.04})(Mg_{0.25}Fe^{2+}_{0.11}Fe^{3+}_{0.12}Al_{1.04}Si_{1.46})O_7$) and $Geh_{48}FGeh_7Åk_{26}FÅk_{19}$ for crystals at 1050 °C (avr. structural formula $(Ca_{1.96}Na_{0.04})(Fe^{3+}_{0.11}Mg_{0.26}Fe^{2+}_{0.19}Al_{0.92}Si_{1.51})O_7$).

Melilite$_{ss}$ crystals in reducing atmosphere at 850 °C have a composition similar to that in oxidation for the same temperature. At 950 °C, the incorporation of Fe^{3+} in the structure is limited (Table 3) and the composition is $Geh_{51}FGeh_1Åk_{27}FÅk_{21}$, with an avr. formula $(Ca_{1.94}Na_{0.05})(Fe^{3+}_{0.01}Mg_{0.25}Fe^{2+}_{0.19}Al_{0.95}Si_{1.56})O_7$. This composition is close to the composition at 1050 °C, which is assumed to be a solid solution between gehlenite and åkermanite-ferroåkermanite (Geh_{53} $Åk_{25}FÅk_{22}$) and is represented by the average formula $(Ca_{1.95}Na_{0.04})(Mg_{0.24}Fe^{2+}_{0.20}Al_{0.97}Si_{1.57})O_7$

(Table 4, Fig. 3d and f). In this work, the co-existence of fassaitic pyroxene and ferrigehlenite-free gehlenite implies that oxygen fugacity is defined by the magnetite stability field, between hematite–magnetite (HM) and quartz-fayalite–magnetite (QFM) equilibriums.

Plagioclase$_{ss}$: Two different types of growth are observed. Plagioclase that grows by a reaction involving dehydroxylated illite, decarbonised calcite and quartz does not have apparent compositional relation with the pre-existing Na-rich plagioclase phenocrysts. Representative analyses of newly formed plagioclase, normalised to 32 oxygens and recalculated to 20 cations are given in Table 5. The composition is distributed within the labradorite and anorthite field ($An_{57–93}$). In oxidising atmosphere the mean value of plagioclase composition is approximately $Ab_{23}An_{71}Or_6$ with an avr. structural formula $(Ca_{0.73}Na_{0.24}K_{0.06}Mg_{0.05})(Si_{2.32}Al_{1.53}Fe^{3+}_{0.08})O_8$. The iron and magnesium contents are quite high, Fe_2O_3 ranges from 1.09 to 3.88 wt% and MgO from 0.00 to 2.22 wt% (Fig. 3c and e). In reduction, chemical composition is $Ab_{20}An_{75}Or_5$ and avr. formula $(Ca_{0.79}Na_{0.19}K_{0.04}Mg_{0.06})(Si_{2.21}Al_{1.65}Fe^{3+}_{0.07})O_8$. Iron and magnesium amounts are also high, Fe_2O_3 ranges between 0.57 and 3.56 wt% and MgO between 0.00 and 2.17 wt% (Fig. 3d and f). The presence of iron and magnesium, even if not common, is compatible with the chemical data available in literature for plagioclases.[31–33] The second composition of plagioclase$_{ss}$ was detected more rarely and mainly in reduction. It grows epitactically at the rim of albite phenocrysts ($Ab_{90}An_8Or_2$) as a solution/precipitation process takes place, where the original Na-rich plagioclase is progressively dissolved with a concurrent formation of a Ca-rich plagioclase ($\sim An_{55}$) and enrichment of the melt with the Ab and Or components. Iron or magnesium has not been detected in the structure of the second type of plagioclase$_{ss}$.

Wollastonite: Aluminium and iron have been detected in the wollastonite crystals, both in oxidising and reducing atmosphere (Table 5, Fig. 3c–f). For oxidising atmosphere the Al_2O_3 content can reach up to 4.61 wt%, whereas in reducing is slightly lower, up to 3.00 wt%. The presence of aluminium may suggest that a limited solid solution of gehlenite in wollastonite takes place.[34,35] The level of iron content remains the same for both atmospheres, having a maximum of 3.00 wt%. The presence of Na, K in the structure is incompatible with the wollastonite structure and is attributed to contamination. The average structural formula, normalized to eighteen oxygens and recalculated to twelve cations, is $(Ca_{0.94}Fe^{2+}_{0.03}Mg_{0.03})(Si_{0.93}Al_{0.08})O_3$ for oxidising and $(Ca_{0.94}Fe^{2+}_{0.03}Mg_{0.03})(Si_{0.96}Al_{0.04})O_3$ for reducing atmosphere.

4. Summary of the results

The data presented in Parts I and II of this work, concerning the macroscopic colour, mineralogy, mineral chemistry and microstructure of the ceramics produced by the Plio-Pleistocene sediments of NW Peloponnese are summarised in Tables 6 and 7, for (in wt%) $5 < CaO < 10$ and $10 < CaO < 15$, respectively. The tables correlate analytical results with expected firing conditions and also provide a first indication for the chemical composition of the raw materials (e.g. a clay with high concentration in CaO or Fe_2O_3). They can be used as reference for future archaeometric investigations upon ceramic findings from excavations in the broader area.

5. Comparison with ancient ceramics

Three representative lamp sherds are used for the comparison study. The colour of lamps' body from macroscopic observation and the concentration (wt%) of the major elements of the fired body are presented in Tables 8 and 9 respectively. The mineralogical composition with the possible firing temperature/atmosphere is given in Table 10, whereas representative chemical compositions of important firing minerals (clinopyroxene$_{ss}$, melilite$_{ss}$) are reported in Table 11. Backscattered electron images are given in Fig. 4 for comparison of the microstructure.

According to the colour of the body, the microstructure, the mineralogy and the chemistry of new minerals such as clinopyroxene$_{ss}$ and melilite$_{ss}$ (Tables 8, 10 and 11 and Fig. 4), both samples PY2 and PY12 have been fired most probably at oxidising atmosphere. The firing temperature of sample PY2 is higher than 900 °C and most probably approximately 950 °C. The firing temperature of sample PY12 is higher than 1000 °C and most probably approximately 1050 °C. Moreover, sample PY12 has been produced by a raw material higher in calcium content, compared to PY2. The decreased amount of the neocrystallised mineral phases wollastonite and gehlenite and of the amorphous phase in ancient samples may be attributed to the burial processes they have been subjected to, that led to the chemical dissolution of the phases.[36–38] This hypothesis is in accordance with the high amount of secondary calcite mainly in the sample PY12 which has been fired at 1050 °C, Table 10. Samples PBY10 have been found at the deposit area and have been considered as discarded by the ancient potter according to the archaeologists. The similar microstructure and mineralogy of PBY10 with the body fired in reduction at 1050 °C (Table 11 and Fig. 4), in combination with the limited number of these ceramic samples, leads to the conclusion that in some cases the potters failed (by accident?) to regulate the firing atmosphere and/or these samples remained at the soaking temperature (1050–1100 °C) for too long.

6. Conclusions

The following conclusions can be drawn:

(a) In oxidising atmosphere and all three firing temperatures, Fe^{3+} incorporates in the structure of fassaite, gehlenite and anorthite. In fassaite, the higher substitution of Fe^{3+} and Al for Mg and Si leads to the increase of esseneite molecule ($CaFe^{3+}AlSiO_6$). In gehlenite, the incorporation of Fe^{3+} increased the amount of ferrigehlenite component, $Ca_2Fe^{3+}_2SiO_7$. Fe^{2+} is mainly entrapped in the structure of wollastonite and at a lesser extent in fassaite and gehlenite.

(b) In reducing atmosphere and 850 °C, the chemical composition of minerals is similar with that in oxidation. At 950 °C, the fassaitic composition of clinopyroxene$_{ss}$ is still preserved but the incorporation of Fe^{3+} in the structure of gehlenite has been limited. At 1050 °C, Fe^{3+} is still present in the structure of anorthite and fassaite, but now Fe^{2+} occupies more sites than Fe^{3+} in clinopyroxene$_{ss}$ and the esseneite component ($CaFe^{3+}AlSiO_6$) is replaced by more hedenbergite component ($CaFe^{2+}Si_2O_6$). On a number of crystals analysed, the esseneite component has been completely replaced by the hedenbergite component forming a new clinopyroxene$_{ss}$ (Al-rich ferroan diopside). In gehlenite, no Fe^{3+} has been detected (absence of ferrigehlenite component, $Ca_2Fe_2^{3+}SiO_7$).

(c) Two tables have been created that correlate in concise manner analytical results with expected firing conditions and provide in addition indications for the chemical composition of the raw materials. This information can be used in future archaeometric investigations upon ceramic findings from excavations in the broader area.

Acknowledgements

Prof. P. Tsolis-Katagas and Assoc. Prof. G.N. Angelopoulos of University of Patras, are gratefully acknowledged for their support during this work. Dr. M. Petropoulos, director of ΛΘ′ Ephorate of Prehistoric and Classical Antiquities, Tripoli, Greece, is thanked with gratitude for providing the ancient sherds. YP is also thankful to the Research Foundation-Flanders (FWO) for the post-doctoral fellowship.

References

1. Petropoulos M. *Roman Lamp Workshops at Patras and the Lychnomanteion*, vol. 70. Athens, Greece: Archaeol. Bulletin, Ministry of Cultural Heritage; 1999.
2. C. Rathossi Ancient ceramics from NW Peloponnese and the provenance of their raw materials: a petrographic, mineralogical, geochemical and archaeometric approach. PhD Thesis. University of Patras, Patras; 2005.
3. Rathossi C, Tsolis-Katagas P, Katagas C. Technology and composition of Roman pottery in northwestern Peloponnese, Greece. *Appl Clay Sci* 2004;**24**(3-4):313–26.
4. Rathossi C, Katagas C, Tsoli-Katagas P. Major and trace element characterization of Archaic and Roman pottery from Achaia, Greece. In: Isabel M, Dias M, Waerenborgh JC, editors. *Understanding people through their pottery, 7th European Meeting on Ancient Ceramic (EMAC'03)*. 2003.
5. Rathossi C, Pontikes Y. Effect of firing temperature and atmosphere on ceramics made of NW Peloponnese clay sediments. Part I: Reaction paths, crystalline phases, microstructure and colour. *J Eur Ceram Soc* 2010;**30**(9):1841–51.
6. Akasaka M, Onuma K. The join rich $CaMgSi_2O_6$–$CaFe^{3+}AlSiO_6$–$CaTiAl_2O_6$ and its bearing on the Ti-rich fassaitic pyroxenes. *Contrib Mineral Petrol* 1980;**71**:301–12.
7. Hijikata K, Okuma K. Phase equilibria of the system $CaMgSi_2O_6$–$CaFe^{3+}AlSiO_6$ in air. *Jpn Assoc Miner Petrol Econ Geol J* 1969;**62**:209–17.
8. Morimoto N. Nomenclature of pyroxenes. *Am Mineral* 1988;**73**:1123–33.
9. Deer WA, Howie RA, Zussman J. *Rock-forming minerals*, vol. 2A, 2nd edition New York: Wiley; 1978. p. 399–414.
10. Cosca MA, Peacor DR. Chemistry and structure of esseneite ($CaFe^{3+}AlSiO_6$), a new pyroxene produced by pyrometamorphism. *Am Mineral* 1987;**72**(1–2):148–56.
11. Coleman LC. Effect of ionic substitution on the unit-cell dimensions of synthetic diopside. *Geol Soc America (Buddington vol)* 1962:422–46.
12. Hijikata K. Unit-cell dimensionw of the clinopyroxenes along the join $CaMgSi_2O_6$–$CaFe^{3+}AlSiO_6$. *J Facul Sci, Hokkaido Univ* 1968;**IV**(14):149–59.
13. Huckenholz HG, Lindhuber W, Springer J. The join $CaSiO_3$–Al_2O_3–Fe_2O_3 of the CaO–Al_2O_3–Fe_2O_3–SiO_2 quaternary system and its bearing on the formation of grandic garnets and fassaitic pyroxene. *Neues Jahrbuch Mineralogie Abhandlungen* 1974;**121**: 160–207.
14. Clark SP, Schairer JF, de Neufville J. Phase relations in the system $CaMgSi_2O_6$–$CaAl_2SiO_6$–SiO_2 at low and high pressure. *Carnegie Inst Wash Yb* 1962;**61**:58–68.
15. Sakata Y. Unit-cell dimensions of synthetic aluminian diopsides. *Jpn J Geol Geogr* 1957;**28**:161–8.
16. Droop GTR. A general equation for estimating Fe^{3+} concentrations in ferromagnesian silicates and oxides from microprobe analyses, using stoichiometric criteria. *Mineral Mag* 1987;**51**(3):431–5.
17. Cawthorn RG, Collerson KD. The recalculation of pyroxene end-member parameters and the estimation of ferrous and ferric iron content from electron microprobe analyses. *Am Mineral* 1974;**59**:1203–8.
18. Oba T, Onuma K. Preliminary report of the join $CaMgSi_2O_6$–$CaFe^{3+}AlSiO_6$ at low oxygen fugacity. *J Fac Sci Hokkaido Univ* 1978;**18**:433–44.
19. Onuma K. Effect of oxygen fugacity on fassaitic pyroxene. *J Fac Sci Hokkaido Univ* 1983;**IV**(20):185–94.
20. Onuma K, Akasaka M, Yagi K. The bearing of the system $CaMgSi_2O_6$–$CaAl_2SiO_6$–$CaFeAlSiO_6$ on fassaitic pyroxene. *LITHOS* 1981;**14**(3):173–82.
21. Onuma K, Yagi K. The join $CaMgSi_2O_6$–$CaAl_2SiO_2O_6$–$CaFe^{3+}AlSiO_6$ in air and its bearing on fassaitic pyroxene. *J Fac Sci Hokkaido Univ* 1975;**IV**(16):343–56.
22. Christie OHJ. On subsolidus relations of silicates. III. A contribution to the chemistry of melilites. *Norsk Geol Tidsskr* 1962;**42**:1–29.
23. Charlu TV, Newton RC, Kleppa OJ. Thermochemistry of synthetic $Ca_2Al_2SiO_7$ (gehlenite)–$Ca_2MgSi_2O_7$ (åkermanite) melilites. *Geochim Cosmochim Acta* 1981;**45**(9):1609–17.
24. Henmi C. Synthesis of bicchulite from gehlenite solid solutions. *Miner J* 1976;**8**(3):171–83.
25. Kimata M, Ii N. The crystal structure of synthetic åkermanite, $Ca_2MgSi_2O_7$. *Neues Jahrb Mineral Monatsh* 1981;**15**:1–10.
26. Kimata M, Ii N. The structural property of synthetic gehlenite, $Ca_2Al_2SiO_7$. *Neues Jahrb Mineral Abh* 1982;**144**:254–67.
27. Merlini M, Gemmi M, Cruciani G, Artioli G. High-temperature behaviour of melilite: in situ X-ray diffraction study of gehlenite–åkermanite–Na melilite solid solution. *Phys Chem Miner* 2008;**35**: 147–55.
28. Andrews KW. The lattice parameters and interplanar spacings of some artificially prepared melilites. *Mineral Mag* 1948;**28**:374–9.
29. Ervin F, Osborn EF. X-ray data of synthetic melilites. *Am Mineral* 1949;**34**:714–22.
30. Neuvonen KJ. Thermochemical investigation of the akermanite–gehlenite series. *Bull Commun Geol Finl* 1952;**152**:1–50.
31. Moroni B, Conti C. Technological features of Renaissance pottery from Deruta (Umbria, Italy): an experimental study. *Appl Clay Sci* 2006;**33**(3–4):230–46.
32. Sugawara T. Thermodynamic analysis of Fe and Mg partitioning between plagioclase and silicate liquid. *Contrib Mineral Petrol* 2000;**138**(2):101–13.
33. Sugawara T. Ferric iron partitioning between plagioclase and silicate liquid: thermodynamics and petrological applications. *Contrib Mineral Petrol* 2001;**141**(6):659–86.
34. Juan VC. The system $CaSiO_3$–$Ca_2Al_2SiO_7$–$NaAlSiO_4$. *J Geol* 1950;**58**:1–15.

35. Yoder Jr HS. Soda melilite. *Carnegie Inst Wash Year Book* 1964;**63**:87–9.
36. Bailey A, Reesman AL. A survey study of the kinetics of wollastonite dissolution in H_2O–CO_2 and buffered systems at 25 °C. *Am J Sci* 1971;**271**:464–72.
37. Xie Z, Walther JV. Dissolution stoichiometry and adsorption of alkali and alkaline earth elements to the acid-reacted wollastonite surface at 25 °C. *Geochim Cosmochim Acta* 1994;**58**(12):2587–98.
38. Heimann RB, Maggetti M. Experiments on simulated burial of calcareous terra sigillata (mineralogical change). Preliminary results. British Museum Occasional Paper 19, London; 1981. p. 163–77.
39. Minguzzi V, Morandi N, Nannetti MC, Pirani R, Poppi L. Mineralogy and geochemistry of the contact minerals in the Predazzo-Monzoni area: Part II. The Predazzo fassaite and revision of the fassaite crystal-chemistry. *Mineral Petrog Acta* 1977;**21**: 189–219.
40. Dondi M, Ercolani G, Fabbri B, Marsigli M. An approach to the chemistry of pyroxenes formed during the firing of Ca-rich silicate ceramics. *Clay Miner* 1998;**33**(2–3):443–52.